





Five-dimensional Poincaré sphere system for representing azimuthally varying vector optical fieldsJia-Hao Zhao,¹ Yue Pan ^{1,*} Xu-Zhen Gao,¹ Rende Ma,¹ Zhong-Xiao Man ¹,
Zhi-Cheng Ren ², Chenghou Tu,³ Yongnan Li,³ and Hui-Tian Wang ^{2,4,†}¹*School of Physics and Physical Engineering, Shandong Provincial Key Laboratory of Laser Polarization and Information Technology, Qufu Normal University, Qufu 273165, China*²*National Laboratory of Solid State Microstructures, School of Physics,**Collaborative Innovation Center of Advanced Microstructures, Nanjing University, Nanjing 210093, China*³*School of Physics, Key Laboratory of Weak-Light Nonlinear Photonics, Nankai University, Tianjin 300071, China*⁴*Collaborative Innovation Center of Extreme Optics, Shanxi University, Taiyuan 030006, China*

(Received 22 April 2022; accepted 21 July 2022; published 4 August 2022)

Vector optical fields (VOFs) with space-variant polarization on the wave front, have attracted considerable attention and have been applied in many realms from focal engineering to light-matter interaction. Recently, some upgraded Poincaré sphere (PS) models have been presented to describe VOFs, providing new insights in studying and applying structured light. Here, we report a model of five-dimensional (5D) PS system consisting of a series of three-dimensional (3D) spheres (Bloch spheres) located on a two-dimensional (2D) plane. In fact, this model is geometrically similar to the solar system, and the 3D Bloch spheres and the 2D plane are analogous to the “planets” and their orbital plane, respectively. This model is the most generalized model describing the azimuthally varying VOFs we know so far. A reliable and flexible experimental scheme is exploited to generate the VOFs represented by the 5D PS system. Furthermore, the 5D PS system is a complete tool to represent the azimuthally varying VOFs with polarization changing along arbitrary circular path on any 3D PS, and can be implemented for representing and designing the spin and orbital angular momenta. The 5D PS system graphically simplifies the representation of complex structured light and provides a prominent toolkit to the design and application of VOFs as well as the corresponding optical angular momentum.

DOI: [10.1103/PhysRevA.106.023506](https://doi.org/10.1103/PhysRevA.106.023506)**I. INTRODUCTION**

As an intrinsic nature of light, polarization plays an important role in engineering optical fields and light-matter interaction. Recently, vector optical fields (VOFs) with space-variant polarization have attracted great attention due to unexpected effects and a myriad of applications [1–3], such as sharper focus beyond diffraction limit [4,5], light needle of a longitudinally polarized field [6,7], quantum optics [8–10], optical information [11–13], optical trapping [14,15], optical imaging [16], nonlinear optics [17], and light-matter interaction [18–20]. With the increasing significance of studying VOFs, it is urgent to propose a complete model for describing the spatial configuration of VOFs, which is helpful in exploring the physical mechanism, novel effects, and applications of VOFs.

For any coherent scalar optical field with space-invariant polarization, its polarization state can be described by a one-to-one point on the traditional Poincaré sphere (PS) model constructed by the Stokes parameters [21]. This basic geometric connection greatly simplifies the polarization representation and becomes a useful tool in dealing with transformation of the polarization state, for instance, such a

traditional PS has been used to explore the geometric phase problem of the optical field [22–24]. Despite its powerful utility, the traditional PS is hard to directly describe the VOFs with space-variant polarization states. In recent years, some upgraded PS models have been presented to represent VOFs, including the hybrid PS [25], higher-order PS [26], hybrid-order PS [27], and generalized PS [28]. These upgraded PS models provide better guidance for further investigation and application of structured light [8,17,29–33]. In the above upgraded PS models, a certain pair of orthogonal bases is used to describe the spatially structured optical fields. In fact, the polarization states of the orthogonal bases can be selected arbitrarily, and this selectivity is an important manipulating degree of freedom which is rarely considered. As a result, a large number of VOFs cannot be represented by the existing models, which limits the design, generation, and application of the structured light. It is worth mentioning that there are also other kinds of upgraded PS models [34–40] for representing different beams instead of VOFs.

Here we aim at constructing the model of five-dimensional (5D) PS system, which is represented by a series of three-dimensional (3D) spheres located on a two-dimensional (2D) plane. In fact, this model is geometrically similar to the solar system, the 3D spheres (Bloch spheres) and the 2D plane are analogous to the “planets” and their orbital plane, respectively. In the 5D PS system, the bases at the north and south poles in each 3D Bloch sphere are the most general orthogonal states

*panyue.89@163.com, panyue@qfnu.edu.cn

†htwang@nju.edu.cn

so far, which have arbitrary spin angular momentum (SAM) and arbitrary orbital angular momentum (OAM). Therefore, this model has more degrees of freedom, which becomes the general model to describe most of the existing VOFs and other new VOFs. A flexible scheme is further proposed to experimentally generate the VOFs represented by the 5D PS system. The 5D PS system can completely represent the azimuthally varying VOFs, and it is introduced to describe and design OAM and SAM. The 5D PS system provides a useful geometric tool for studying VOFs and optical angular momenta, which can be applied in many realms.

II. THEORY AND DESCRIPTION

As is well known, any polarization state can be represented by the weighted superposition of two orthogonal basis states. Thus, the optical field can be represented as

$$|\psi\rangle = \psi_N^m |N_r^{m\theta}\rangle + \psi_S^m |S_r^{m\theta}\rangle. \quad (1)$$

The optical field carrying OAM can be expressed as the superposition of the spiral harmonics $\exp(jm\phi)$. For the VOF described by the 5D PS system we propose here, $|N_r^{m\theta}\rangle$ and $|S_r^{m\theta}\rangle$ are two orthogonal bases carrying opposite SAMs and OAMs as

$$\begin{aligned} |N_r^{m\theta}\rangle &= e^{-jm\phi} [\cos(\pi r)\hat{\mathbf{e}}_l - \sin(\pi r)e^{-j\theta}\hat{\mathbf{e}}_r], \\ |S_r^{m\theta}\rangle &= e^{+jm\phi} [\sin(\pi r)e^{+j\theta}\hat{\mathbf{e}}_l + \cos(\pi r)\hat{\mathbf{e}}_r], \end{aligned} \quad (2)$$

where ϕ is the azimuthal coordinate and $\pm m$ are the topological charges of the vortices carried by the two bases. r determines the ellipticities of the orthogonal bases, and the ellipticities change continuously within a range of $[-1, 1]$ when $r \in [0.5, 1]$. θ controls the orientations of the polarization ellipses of the orthogonal bases within a range of $\theta \in [0, 2\pi)$. Specifically, the orientations of the two bases are $\theta/2$ and $\theta/2 + \pi/2$ and change continuously within ranges of $[0, \pi)$ and $[\pi/2, 3\pi/2)$, respectively. ψ_N^m and ψ_S^m in Eq. (1) represent the weights of the orthogonal bases $|N_r^{m\theta}\rangle$ and $|S_r^{m\theta}\rangle$, which can be expressed as

$$\begin{aligned} \psi_N^m &= \sin(\alpha + \pi/4)e^{-j\varphi}, \\ \psi_S^m &= \cos(\alpha + \pi/4)e^{+j\varphi}, \end{aligned} \quad (3)$$

where α determines the relative intensity fraction and φ controls the phase difference between the orthogonal bases. 2α and 2φ vary within the ranges of $[-\pi/2, \pi/2]$ and $[0, 2\pi)$, respectively. Therefore, in this 5D PS system, the orthogonal bases are the most general so far.

It can be seen that the optical fields in the model of the 5D PS system are represented by five parameters including $(m, \theta; r, 2\alpha, 2\varphi)$. Referencing [21,26,28], the parameters $(r, 2\alpha, 2\varphi)$ are used to construct the 3D Bloch sphere. Due to the 3D limit of the Bloch space, the model of the 5D PS system with five parameters cannot be represented by a single Bloch sphere. We further construct a 2D polar coordinate plane with the two parameters (m, θ) , where θ is the azimuthal coordinate within a range of $[0, 2\pi)$, and $m \geq 0$ is the radial coordinate (but m is a discrete natural number instead of all non-negative real number). Thus, the 5D PS system is constructed by a series of planets (3D Bloch spheres) located at different discrete ‘‘orbits’’ on the 2D plane. The

polar coordinates (m, θ) on the 2D plane defines the orbit location of a planet (3D Bloch sphere) with the three parameters $(r, 2\alpha, 2\varphi)$, and accordingly, we label this Bloch sphere as an $m\theta$ sphere. In this way, the model of 5D PS system has been established mathematically as shown in Fig. 1.

Referencing the definition of the Stokes parameters [21,26,28], we calculate the Stokes parameters of the $m\theta$ sphere in the 5D PS system as

$$\begin{aligned} G_0^{m\theta} &= (|N_r^{m\theta}\langle\psi\rangle|^2 + |S_r^{m\theta}\langle\psi\rangle|^2)r = r, \\ G_1^{m\theta} &= 2 \operatorname{Re}(\langle N_r^{m\theta}\langle\psi\rangle^* | S_r^{m\theta}\langle\psi\rangle \rangle)r = r \cos 2\alpha \cos 2\varphi, \\ G_2^{m\theta} &= 2 \operatorname{Im}(\langle N_r^{m\theta}\langle\psi\rangle^* | S_r^{m\theta}\langle\psi\rangle \rangle)r = r \cos 2\alpha \sin 2\varphi, \\ G_3^{m\theta} &= (|N_r^{m\theta}\langle\psi\rangle|^2 - |S_r^{m\theta}\langle\psi\rangle|^2)r = r \sin 2\alpha. \end{aligned} \quad (4)$$

Obviously, the expressions of parameters $G_1^{m\theta}$, $G_2^{m\theta}$, and $G_3^{m\theta}$ agree with the Cartesian coordinates of the sphere with a radius of $G_0^{m\theta}$. Hence, we use $G_1^{m\theta}$, $G_2^{m\theta}$, and $G_3^{m\theta}$ to describe the $m\theta$ sphere, and $(r, 2\alpha, 2\varphi)$ are the corresponding spherical coordinates, which can be given by

$$\begin{aligned} r &= G_0^{m\theta}, \\ \sin 2\alpha &= G_3^{m\theta} / G_0^{m\theta}, \\ \tan 2\varphi &= G_2^{m\theta} / G_1^{m\theta}, \end{aligned} \quad (5)$$

where r , 2α , and 2φ represent the radius, latitude, and longitude of each $m\theta$ sphere. The orbit location of each $m\theta$ sphere is determined by the coordinates (m, θ) . The five coordinates $(m, \theta; r, 2\alpha, 2\varphi)$ can define the maximum amount of azimuthally varying VOFs so far. Especially, the points on the $G_3^{m\theta}$ axis of each $m\theta$ sphere represent a series of scalar vortex fields with continuously varying SAM. Of course, the scalar field with spatially invariant polarization can be regarded as a special case of the VOF.

The schematic of the 5D PS system is shown in Fig. 1 where three white circles show the orbits with topological charges of $m = 1-3$, respectively. Figures 1(a)–1(d) show the $m\theta$ spheres with coordinates $(m, \theta) = (1, \pi/2)$, $(1, 0)$, $(2, 3\pi/2)$, and $(2, 7\pi/4)$, respectively. It can be seen from Fig. 1 that the coordinate m represents the number of the polarization changing periods along azimuthal direction on the wave front of the VOF, and the case for θ is more complicated. When m is fixed and θ is changeable, the polarization states of the VOFs on the outer spherical shell with $r = 1$ do not change as shown in the $m\theta$ sphere with $(r, 2\alpha, 2\varphi) = (1, 0, \pi/2)$ in Figs. 1(a)–1(d). This originates from the fact that θ has no influence when $r = 1$, which can be easily understood from Eqs. (1) and (2). For the inner spherical shell with $r = 0.5$, the orientation of the polarization state of the VOF rotates counterclockwise by θ , compared with the VOF in the $m\theta$ sphere when $\theta = 0$ as shown in Figs. 1(a) and 1(b). When $r \in (0.5, 1)$, different values of θ mean different kinds of orthogonal bases, leading to the VOFs with different polarization distributions. As a result, the 5D PS system can describe more kinds of azimuthally varying VOFs. Now we discuss the relation between the 5D PS system and the former created PS models. The $m\theta$ sphere degenerates into the traditional generalized PS [28] when $\theta = 3\pi/2$, and the 5D PS system with $\theta = 3\pi/2$ is a series of generalized PSs with different topological charges m . When $r = 0.5$ and 1, the $m\theta$

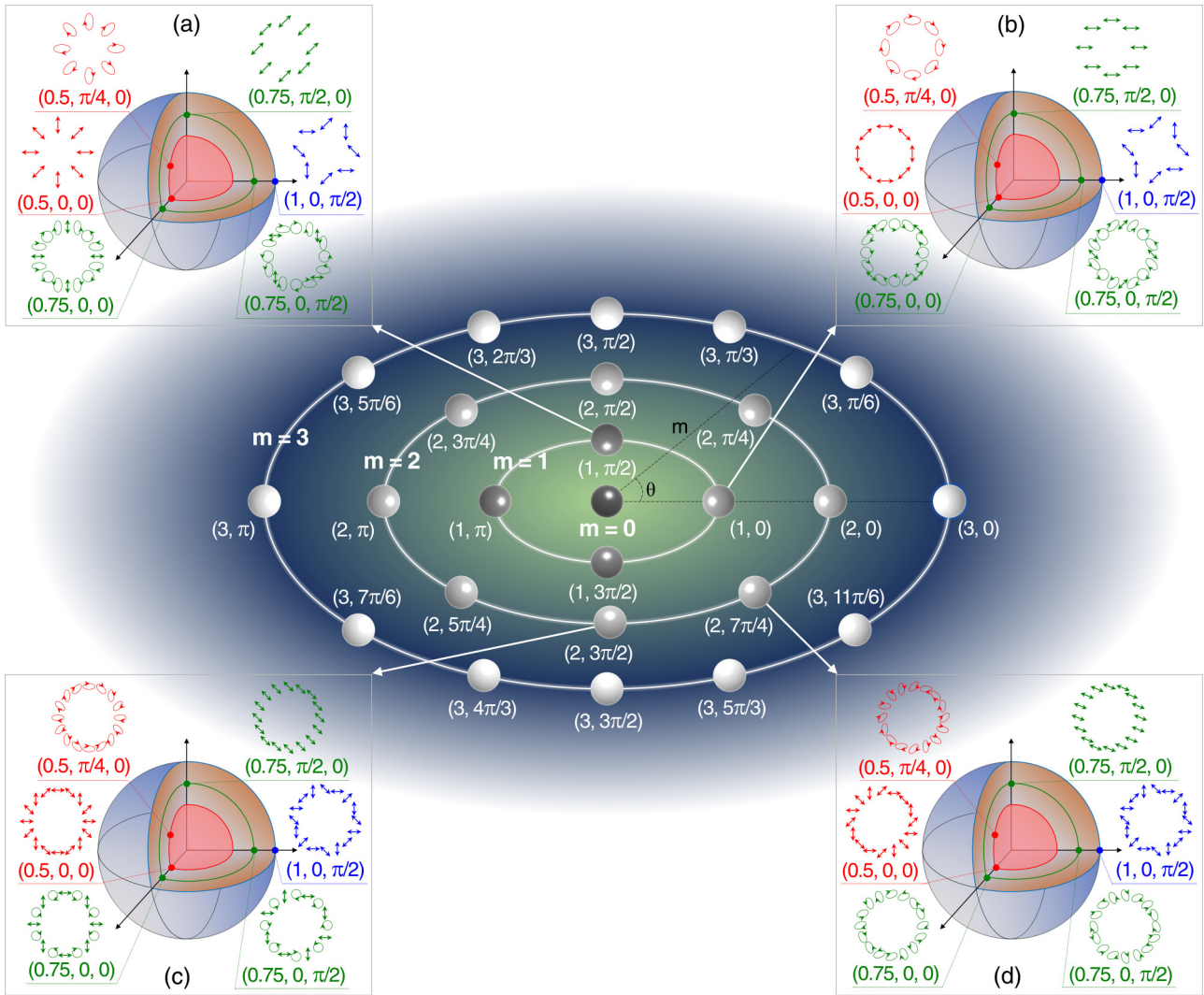


FIG. 1. The schematic of the 5D PS system. The plane is with polar coordinates (m, θ) , and each point on the plane represents an $m\theta$ sphere. The white circles represent the orbits with $m = 1-3$, respectively. (a)–(d) show the $m\theta$ spheres with coordinates of $(m, \theta) = (1, \pi/2)$, $(1, 0)$, $(2, 3\pi/2)$, and $(2, 7\pi/4)$. The polarization states of several VOFs in these $m\theta$ spheres are shown with the parameters $(r, 2\alpha, 2\varphi)$.

sphere further degenerates into the outer sphere surfaces of the higher-order PS [26] and hybrid PS [25] with a geometric rotation of the sphere. Thus, the 5D PS system contains all the cases of the fully polarized VOFs in these two models. When $m = 0$ and $r = 0.5$, the $m\theta$ sphere in the center of the (m, θ) plane degenerates into the outer sphere surface of the traditional PS [21], which can characterize the scalar optical fields with different polarizations. We should point out that although we have designed the 5D PS system with discrete orbits, the radius m in this model can be any values including nonintegers for different needs. For the case of noninteger m , the bases in Eq. (2) cannot be considered as the eigenstates of OAM. Even so, the optical field can still be described by Eqs. (1)–(3) and by the 5D PS system.

III. EXPERIMENTAL SETUP AND RESULTS

Figure 2 depicts the experimental setup we propose for generating the VOFs represented in the 5D PS system, and the main configuration is a $4f$ system composed of a pair of

identical lenses (L1 and L2). The input horizontally polarized optical field is incident on a cosine grating displayed on a SLM, and the transmission function of the grating is $t(x, y) = 0.5 + 0.5 \cos(2\pi f_0 x + \delta)$, where f_0 is the spatial frequency.

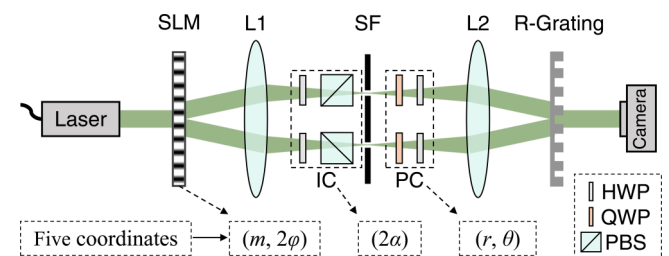


FIG. 2. Schematic of the experimental setup. SLM: spatial light modulator; L1 and L2: pair of lenses; SF: spatial filter; IC: intensity controller; PC: polarization controller; QWP: quarter-wave plate; HWP: half-wave plate; PBS: polarizing beam splitter; R-Grating: Ronchi phase grating. The coordinates $(m, 2\theta)$, 2α , and (r, θ) in the 5D PS system are modulated by the SLM, IC, and PC, respectively.

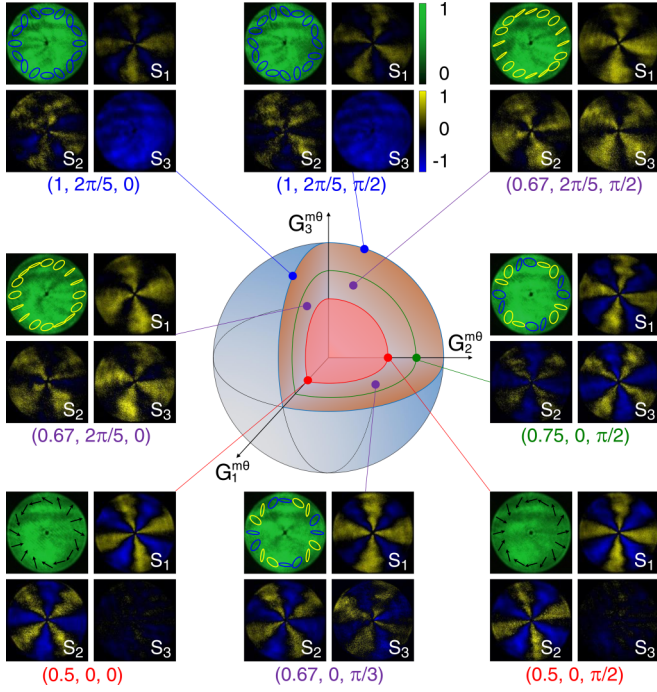


FIG. 3. Experimentally measured VOFs in the $m\theta$ spheres with $(m, \theta) = (2, \pi/3)$ in the 5D PS system. The spherical coordinates of the eight VOFs are $(r, 2\alpha, 2\varphi) = (1, 2\pi/5, 0)$, $(1, 2\pi/5, \pi/2)$, $(0.67, 2\pi/5, \pi/2)$, $(0.75, 0, \pi/2)$, $(0.5, 0, \pi/2)$, $(0.67, 0, \pi/3)$, $(0.5, 0, 0)$, and $(0.67, 2\pi/5, 0)$, respectively. For each VOF, the four pictures show the total intensity and polarization distributions, Stokes parameters S_1 , S_2 , and S_3 , respectively.

When we set $\delta = m\phi + \varphi$, the input field is split into ± 1 orders carrying opposite phase distributions of $\pm(m\phi + \varphi)$, corresponding to Eqs. (2) and (3). The two orders are allowed to pass through a SF, and the relative intensity of the two orders is controlled by the IC composed of two HWPs and two PBSs. The modulation of the intensities of the two orders is equivalent to adjust the parameter α in Eq. (3). Then the two orders are converted into two orthogonally polarized beams by the PC, which is composed of two QWPs and two HWPs. The PC with four wave plates can guarantee that the two orders are orthogonally polarized with arbitrary polarizations, corresponding to the modulation of the parameters (r, θ) in Eq. (2). The two orthogonally polarized orders with controllable intensity distribution are recombined by the Ronchi phase grating placed in the output plane of the $4f$ system. The experimentally generated VOF is detected by a camera on the image plane of the SLM. It should be pointed out that the experimental setup with SLM and the $4f$ system is commonly used in generating VOFs [14,41], but the method we introduce here is more flexible with IC and PC inserted as more degrees of freedom can be manipulated in the experiment. In this way, the setup can generate all the VOFs in the 5D PS system completely, and all five coordinates are modulated independently, leading to the possibility of flexible transformation of the VOFs in the 5D PS system in the experiment.

Figure 3 shows the experimentally generated VOFs in the $m\theta$ sphere with coordinates $(m, \theta) = (2, \pi/3)$ in the 5D PS system. The spherical coordinates of the eight

VOFs are $(r, 2\alpha, 2\varphi) = (1, 2\pi/5, 0)$, $(1, 2\pi/5, \pi/2)$, $(0.67, 2\pi/5, \pi/2)$, $(0.75, 0, \pi/2)$, $(0.5, 0, \pi/2)$, $(0.67, 0, \pi/3)$, $(0.5, 0, 0)$, and $(0.67, 2\pi/5, 0)$, respectively. With the coordinates of $(r, 2\alpha, 2\varphi) = (0.5, 0, 0)$ and $(0.5, 0, \pi/2)$, the two points are located on the equatorial plane of the inner spherical shell of $r = 0.5$, and the corresponding VOFs are common local linearly polarized VOFs [41], which can be proved by the zero Stokes parameter S_3 shown in Fig. 3. When $(r, 2\alpha, 2\varphi) = (1, 2\pi/5, 0)$ and $(1, 2\pi/5, \pi/2)$, the two points are located on the outer spherical shell of $r = 1$. The corresponding VOF is a left-handed elliptically polarized VOF, which has the space-invariant ellipticity but the space-variant orientations. Thus, the Stokes parameters S_1 and S_2 are space variant, and S_3 is uniform on the wave front. Obviously, when $r = 0.5$ and 1 , the two bases in Eq. (2) are circularly polarized, and the ellipticities of the polarizations on the wave front of the VOFs are space invariant. If $r \in (0.5, 1)$, the ellipticities of the polarizations will be space variant. For the points with coordinates of $(r, 2\alpha, 2\varphi) = (0.67, 2\pi/5, 0)$ and $(0.67, 2\pi/5, \pi/2)$, the polarizations on the wave front are purely right handed with space-variant ellipticities, so the Stokes parameter S_3 is space variant with positive values. For the VOFs with $(r, 2\alpha, 2\varphi) = (0.75, 0, \pi/2)$ and $(0.67, 0, \pi/3)$, right- and left-handed elliptic polarizations can be found on the wave front, so the Stokes parameter S_3 is space variant with both positive and negative values. The experimental results in Fig. 3 are in good agreement with the simulated polarization distributions.

IV. REPRESENTATION OF THE AZIMUTHALLY VARYING VOFs

As introduced above, VOFs have attracted extensive attention [1–3] due to the unique space-variant polarization, intriguing features, and extensive applications. Among various VOFs reported in literature, the most common and widely applied ones are the azimuthally varying VOFs, such as the radially polarized VOF [4–7,12,13,18,41], azimuthally polarized VOF [5,13,41], hybridly polarized VOF [12], and VOFs in the hybrid PS, higher-order PS, hybrid-order PS, and generalized PS [8,17,25–33]. All the VOFs mentioned above have a common feature that the azimuthally varying polarization changes along the circular paths on the traditional PS, and most of the paths correspond to the longitude or latitude on the sphere. The hybrid PS, higher-order PS, hybrid-order PS, and generalized PS can describe these azimuthally varying VOFs. However, there is no model to describe the azimuthally varying VOFs with polarization changing along arbitrary circular paths on the PS. The 5D PS system we propose can represent all these VOFs completely, which also provides one representative application for this model. The detailed derivation will be presented below.

As we know, the polarization of a scalar optical field can be represented by a point $(2\alpha_1, 2\varphi_1)$ on the PS as shown in Figs. 4(a1) and 4(a2), and the expression of the optical field is

$$\mathbf{E}_1 = \begin{bmatrix} Ae^{-j\varphi_1} + Be^{j\varphi_1} \\ jAe^{-j\varphi_1} - jBe^{j\varphi_1} \end{bmatrix}, \quad (6)$$

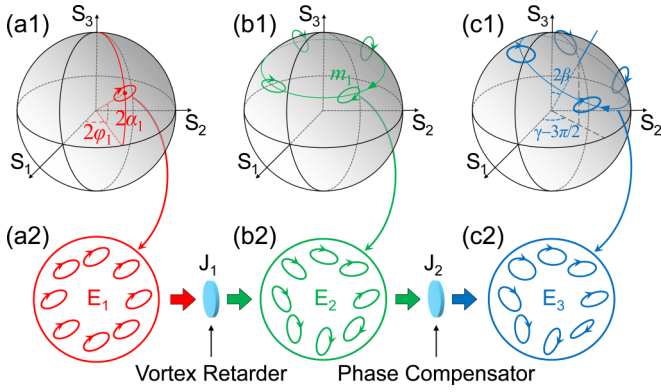


FIG. 4. The schematic of deducing the azimuthally varying VOF whose polarization corresponds to arbitrary circular path on the PS. (a1) and (a2) A point with coordinates $(2\alpha_1, 2\varphi_1)$ on the PS and the polarization state of the corresponding scalar optical field. (b1) and (b2) The latitude circle on the PS and the corresponding VOF after inserting a vortex retarder with the Jones matrix of \mathbf{J}_1 . (c1) and (c2) The arbitrary circular path on the PS and the corresponding VOF after inserting a phase compensator with Jones matrix of \mathbf{J}_2 .

with

$$A = \frac{1}{\sqrt{2}} \sin(\alpha_1 + \pi/4), \quad B = \frac{1}{\sqrt{2}} \cos(\alpha_1 + \pi/4), \quad (7)$$

where α_1 and φ_1 vary in the ranges of $[-\pi/4, \pi/4]$ and $(0, \pi]$, respectively.

We assume that the scalar optical field passes through a vortex retarder [42], which is designed by analogy to a $1/2$ wave plate with the continuously changing angle of $m_1\phi/2$ between the fast axis and the horizontal direction. The Jones matrix of the vortex retarder is

$$\mathbf{J}_1 = \begin{bmatrix} \cos(m_1\phi) & \sin(m_1\phi) \\ -\sin(m_1\phi) & \cos(m_1\phi) \end{bmatrix}, \quad (8)$$

where ϕ is the azimuthal coordinate and m_1 is the topological charge varying in range of $[0, +\infty)$. Therefore, the optical field passing through the vortex retarder can be expressed as

$$\mathbf{E}_2 = \mathbf{J}_1 \mathbf{E}_1 = \begin{bmatrix} Ae^{-j(\varphi_1 - m_1\phi)} + Be^{j(\varphi_1 - m_1\phi)} \\ jAe^{-j(\varphi_1 - m_1\phi)} - jBe^{j(\varphi_1 - m_1\phi)} \end{bmatrix}. \quad (9)$$

Compared with Eq. (6), the polarization state of the optical field \mathbf{E}_2 can be represented by the points $(2\alpha_1, 2\varphi_1 - 2m_1\phi)$ on the PS surface, and the variable ϕ is the azimuthal coordinate on the wave front of \mathbf{E}_2 . This means that the polarization state on the wave front of the optical field \mathbf{E}_2 is changeable along the arbitrary latitude circle on the PS as shown in Fig. 4(b1), and the optical field \mathbf{E}_2 is a VOF with space-variant polarization as shown in Fig. 4(b2). Thus, the ellipticity of the polarization state of the optical field \mathbf{E}_2 is space invariant, but the orientation of polarization rotates clockwise from φ_1 to $\varphi_1 - m_1\phi$. The position of the starting point (corresponding to the position of $\phi = 0$ on the wave front) of the circular path is determined by $(2\alpha_1, 2\varphi_1)$. The topological charge m_1 determines the number of the polarization changing periods, which also indicates the number of turns that the polarization changes around the circular path on the PS.

Then, the optical field \mathbf{E}_2 passes through a phase compensator with a phase delay of 2β and an angle of $\gamma/2$ between the fast axis and the horizontal axis, and β and γ vary in the ranges of $[0, \pi/2]$ and $[0, 2\pi)$, respectively. According to Ref. [43], the circular path in Fig. 4(b1) will rotate after inserting the phase compensator. The central axis of the rotated circular path has the spherical coordinates $(2\beta, \gamma + \pi/2)$ when $\gamma \in [0, 3\pi/2)$ and $(2\beta, \gamma - 3\pi/2)$ when $\gamma \in [3\pi/2, 2\pi)$ as shown in Fig. 4(c1). The Jones matrix of the phase compensator can be written as [43]

$$\mathbf{J}_2 = \begin{bmatrix} \cos \beta + j \sin \beta \cos \gamma & j \sin \beta \sin \gamma \\ j \sin \beta \sin \gamma & \cos \beta - j \sin \beta \cos \gamma \end{bmatrix}. \quad (10)$$

Therefore, the optical field can be expressed as

$$\begin{aligned} \mathbf{E}_3 &= \mathbf{J}_2 \mathbf{E}_2 \\ &= \begin{bmatrix} (C + D) \cos \beta + j(Ce^{+j\gamma} + De^{-j\gamma}) \sin \beta \\ j(C - D) \cos \beta + (Ce^{+j\gamma} - De^{-j\gamma}) \sin \beta \end{bmatrix}, \end{aligned} \quad (11)$$

with

$$C = Ae^{-j(\varphi_1 - m_1\phi)}, \quad D = Be^{j(\varphi_1 - m_1\phi)}. \quad (12)$$

Affected by the phase compensator, the polarization state of the VOF is along arbitrary circular path on the PS as shown in Figs. 4(c1) and 4(c2). As a result, Eq. (11) can describe the azimuthally varying VOFs whose polarization corresponds to an arbitrary circular path on the PS.

Now we need to prove that the VOF in the 5D PS system is the same as the optical field \mathbf{E}_3 in Eq. (11). Comparing Eqs. (1)–(3) and (11), we can find that expressions of the two optical fields are the same if we set $m_1 = m$, $\alpha_1 = -\alpha$, $\varphi_1 = -\varphi + \pi$, $\beta = \pi - \pi r$, $\gamma = \theta + \pi/2$ when $\theta \in [0, 3\pi/2)$ and $\gamma = \theta - 3\pi/2$ when $\theta \in [3\pi/2, 2\pi)$. Thus, the 5D PS system with the five coordinates $(m, \theta; r, 2\alpha, 2\varphi)$ can describe the azimuthally varying VOFs with polarization changing along arbitrary circular path on the PS. $(2\alpha, 2\varphi)$ determine the starting point of the circular path on the PS, and (θ, r) determine the rotation of the circular path. The value of the topological charge m determines the number of turns that the polarizations change around the circular path on the PS. In this way, the 5D PS system can completely represent all the azimuthally varying VOFs with polarization changing along arbitrary circular paths on the PS. This means that the 5D PS system can describe most of the existing VOFs and other new VOFs.

V. DISCUSSION OF OAM AND SAM

The OAM and SAM are two important inherent features of light, which have attracted great attention in recent years [2,3,44–52]. The intrinsic OAM is related to the vortex phase of structured light which can make particles orbit around the beam axis, whereas the SAM is associated with the circular polarization which has two possible quantized values of $\pm\hbar$. The SAM for the scalar optical field can be described simply by the traditional PS [21], whereas the OAM can be represented by a so-called orbital PS [53]. Recently, the optical angular momenta of VOFs have been studied by the upgraded PS models [25–33], opening new avenues for studying and applying optical angular momentum. Compared with the former upgraded PS models, the 5D PS system we developed can

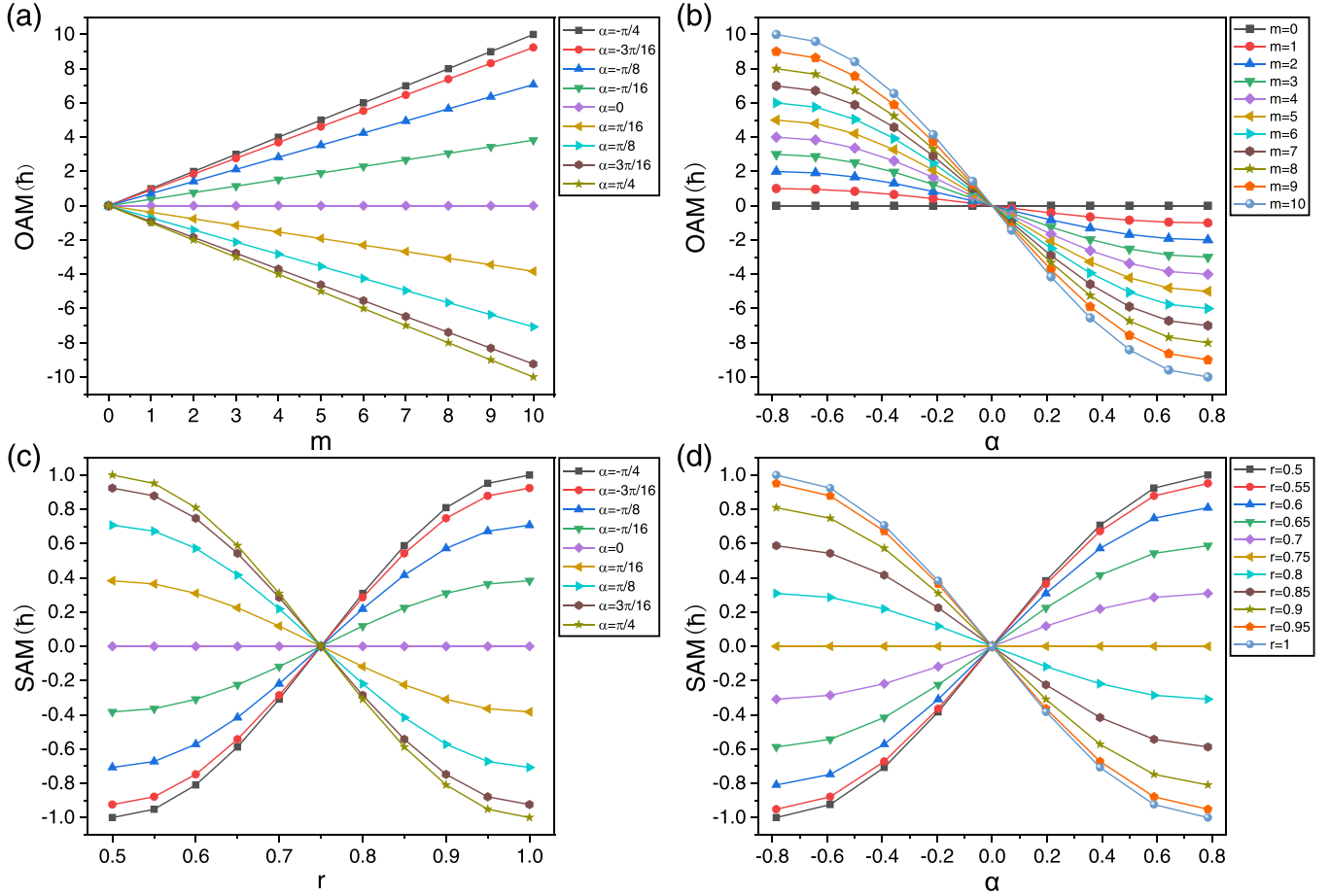


FIG. 5. The OAM and average SAM per photon for the VOFs in the 5D PS system. (a) and (b) show the dependences of the OAM on m and α , (c) and (d) show the dependences of the average SAM per photon on r and α when m is a nonzero integer, respectively.

represent more kinds of OAM and SAM for the VOF, which may be used in many realms.

Based on Eqs. (1)–(3), the OAM per photon for the VOF in the 5D PS system is represented as [14,54]

$$\begin{aligned} J^o &= \hbar \operatorname{Im}(E_x^* \partial E_x / \partial \phi + E_y^* \partial E_y / \partial \phi) \\ &= -m\hbar \sin(2\alpha), \end{aligned} \quad (13)$$

where E_x and E_y are the x and y components of the electric field of the VOF. We can see that m and α determine the OAM, and the OAM per photon can be arbitrarily manipulated within a range of $[-m\hbar, m\hbar]$ by adjusting the value of α .

The average SAM per photon for the VOF is calculated by [55]

$$J^s = \hbar\omega \mathcal{M}_{zz}^s / \mathcal{F}, \quad (14)$$

where ω is angular frequency of the optical field and \mathcal{M}_{zz}^s and \mathcal{F} are the average SAM flow and the energy flow of the VOF, respectively. Combined with Eqs. (1)–(3) and (14), the average SAM per photon for the VOF in the 5D PS system is

$$\begin{aligned} J^s &= -\hbar \{ \sin(2\alpha) \cos(2\pi r) + \cos(2\alpha) \sin(2\pi r) \\ &\quad \times [\sin(4m\pi + 2\varphi + \theta) - \sin(2\varphi + \theta)] / 4\pi m \}. \end{aligned} \quad (15)$$

When m is a nonzero integer, Eq. (15) can be simplified as

$$J^s = -\hbar \sin(2\alpha) \cos(2\pi r). \quad (16)$$

In this way, the average SAM for the VOF in the 5D PS system is only related to r and α .

Figure 5 shows the OAM and the average SAM for the VOFs in the 5D PS system. Figures 5(a) and 5(b) show the dependences of the OAM on m and α , respectively. When $m = 0$ or $\alpha = 0$, the OAM for the VOF is zero according to Eq. (13). The corresponding optical field is a scalar optical field with the space-invariant phase when $m = 0$, whereas the VOF is superposed by the orthogonal bases with the opposite OAMs and equal intensity when $\alpha = 0$. The OAM is a linear function of m and a sine function of α as shown in Fig. 5 and Eq. (13). Figures 5(c) and 5(d) show the dependences of the average SAM per photon on r and α , respectively. The SAM is a cosine function of r and a sine function of α as shown in Eq. (16) where the SAM will be zero when $r = 0.75$ or $\alpha = 0$. We can see from Fig. 5 that the VOFs described by the 5D PS system can carry the OAM or average SAM with arbitrary value. It should be pointed out that for the case when m is a noninteger, the OAM and average SAM can also be calculated by Eqs. (13) and (15).

Obviously, the 5D PS system can be used to design optical fields with the arbitrary combination of OAM and SAM, and the corresponding design procedure is described by the flow chart in Fig. 6. First, we should input the initial values of the OAM J^o and the average SAM per photon J^s . Then the condition $|J^s|/\hbar \leq |J^o|/|J^o|$ is used to judge whether the

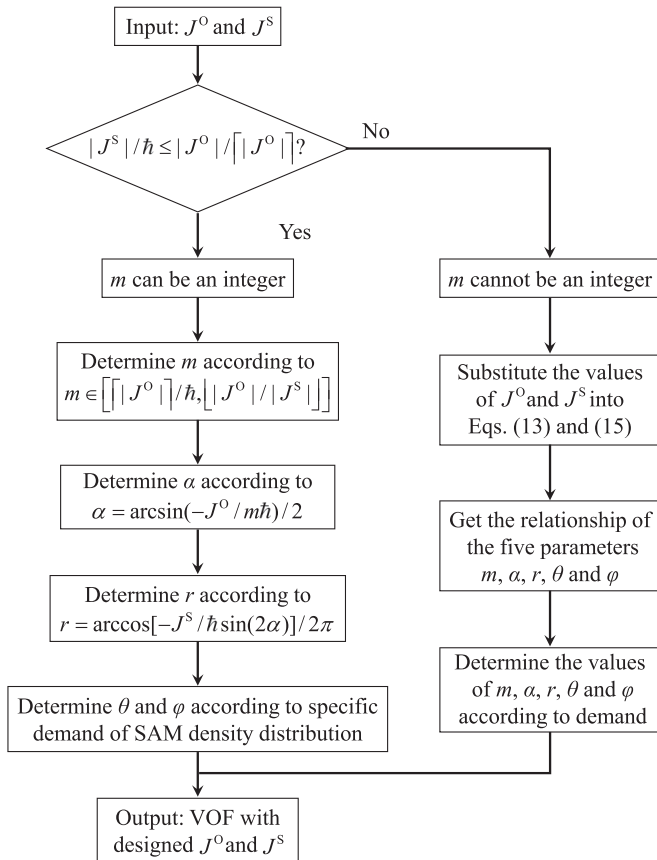


FIG. 6. Flow chart of design procedure of the VOF with arbitrary combination of OAM and SAM.

value of m is an integer or not, where $\lceil \cdot \rceil$ is a ceiling function with $\lceil x \rceil = \min\{n \in \mathbf{Z}: x \leq n\}$. If the inequation is satisfied, the value of m can be an integer according to Eqs. (13) and (15). Otherwise, the value of m cannot be an integer. If m can be an integer, the value of m is determined by $m \in [\lceil |J^o| \rceil / \hbar, \lfloor |J^o| / |J^s| \rfloor]$, where $\lfloor \cdot \rfloor$ is a floor function with $\lfloor x \rfloor = \max\{n \in \mathbf{Z}: n \leq x\}$. According to the values of J^o and m , the value of α is calculated by $\alpha = \arcsin(-J^o/m\hbar)/2$. The value of r is obtained by $r = \arccos[-J^s/\hbar \sin(2\alpha)]/2\pi$ based on the values of J^s and α . In addition, the values of θ and φ can be derived by the specific demand of the SAM density distribution. If m cannot be an integer, the values of the five parameters $(m, \theta; r, 2\alpha, 2\varphi)$ are calculated by Eqs. (13)

and (15) based on J^o and J^s . At last, the VOFs in the 5D PS system with the arbitrary combination of OAM and SAM can be achieved according to the five calculated parameters $(m, \theta; r, 2\alpha, 2\varphi)$.

VI. CONCLUSION

In conclusion, we have presented a model of 5D PS system as a geometric representation of the azimuthally varying VOFs. The 5D PS system is constructed by the orthogonal bases with the continuously changeable orientation of the polarization ellipse, continuously changeable ellipticity (corresponding to arbitrary SAM), and high-dimensional OAM. In this way, the 5D PS system is designed with five dimensions, represented by a series of 3D Bloch spheres located on a 2D plane, similar to the solar system with the 3D planets and their 2D orbital plane. Hence, as far as we know, the 5D PS system constructed in a 5D space is the most general model to describe the azimuthally varying VOFs. In addition, an alternative experimental method is proposed to generate the VOFs in the 5D PS system, and all the five parameters in the model can be flexibly changed or selected in the experiment. It is also proved that the 5D PS system can completely represent the azimuthally varying VOFs with polarization changing along the arbitrary circular paths on the traditional PS. This not only means that most of the VOFs in the previous researches can be represented by this model, but also indicates that the 5D PS system provides the scheme to design new VOFs, which greatly enriches the family of VOFs. Furthermore, the 5D PS system is introduced to represent and design OAM and SAM, opening new avenues for studying and applying optical angular momentum. The theoretical and experimental methods in this paper can be used to describe, design, generate, and apply VOFs in many realms.

ACKNOWLEDGMENTS

We acknowledge support from the National Natural Science Foundation of China (Grants No. 11804187, No. 11904199, No. 11974209, No. 11922406, No. 12074196, No. 12074197, and No. 12174217), the Taishan Scholar Project of Shandong Province (Grant No. tsqn201812059), the China Postdoctoral Science Foundation (Grant No. 2020M682142), the Natural Science Foundation of Shandong Province (Grant No. ZR2019BF006).

[1] Q. Zhan, *Adv. Opt. Photonics* **1**, 1 (2009).
 [2] H. Rubinsztein-Dunlop, A. Forbes, M. V. Berry, M. R. Dennis, D. L. Andrews, M. Mansuripur, C. Denz, C. Alpmann, P. Banzer, T. Bauer *et al.*, *J. Opt.* **19**, 013001 (2017).
 [3] A. Forbes, M. de Oliveira, and M. R. Dennis, *Nat. Photonics* **15**, 253 (2021).
 [4] R. Dorn, S. Quabis, and G. Leuchs, *Phys. Rev. Lett.* **91**, 233901 (2003).
 [5] X. Xie, Y. Chen, K. Yang, and J. Zhou, *Phys. Rev. Lett.* **113**, 263901 (2014).

[6] H. Wang, L. Shi, B. Lukyanchuk, C. Sheppard, and C. T. Chong, *Nat. Photonics* **2**, 501 (2008).
 [7] H. Hu, Q. Gan, and Q. Zhan, *Phys. Rev. Lett.* **122**, 223901 (2019).
 [8] V. Parigi, V. D'Ambrosio, C. Arnold, L. Marrucci, F. Sciarrino, and J. Laurat, *Nat. Commun.* **6**, 7706 (2015).
 [9] B. Ndagano, B. Perez-Garcia, F. S. Roux, M. McLaren, C. Rosales-Guzman, Y. Zhang, O. Mouane, R. I. Hernandez-Aranda, T. Konrad, and A. Forbes, *Nat. Phys.* **13**, 397 (2017).

- [10] A. Sit, F. Bouchard, R. Fickler, J. Gagnon-Bischoff, H. Larocque, K. Heshami, D. Elser, C. Peuntinger, K. Günthner, B. Heim *et al.*, *Optica* **4**, 1006 (2017).
- [11] X. Li, T. H. Lan, C. H. Tien, and M. Gu, *Nat. Commun.* **3**, 998 (2012).
- [12] Y. Chen, K. Y. Xia, W. G. Shen, J. Gao, Z. Q. Yan, Z. Q. Jiao, J. P. Dou, H. Tang, Y. Q. Lu, and X. M. Jin, *Phys. Rev. Lett.* **124**, 153601 (2020).
- [13] Z. Zhu, M. Janasik, A. Fyffe, D. Hay, Y. Zhou, B. Kantor, T. Winder, R. W. Boyd, G. Leuchs, and Z. Shi, *Nat. Commun.* **12**, 1666 (2021).
- [14] X. L. Wang, J. Chen, Y. Li, J. Ding, C. S. Guo, and H. T. Wang, *Phys. Rev. Lett.* **105**, 253602 (2010).
- [15] Y. Yang, Y. Ren, M. Chen, Y. Arita, and C. Rosales-Guzmán, *Adv. Photonics* **3**, 034001 (2021).
- [16] G. Bautista, J. Mäkitalo, Y. Chen, V. Dhaka, M. Grasso, L. Karvonen, H. Jiang, M. J. Huttunen, T. Huhtio, H. Lipsanen *et al.*, *Nano Lett.* **15**, 1564 (2015).
- [17] H. J. Wu, B. S. Yu, Z. H. Zhu, W. Gao, D. S. Ding, Z. Y. Zhou, X. P. Hu, C. Rosales-Guzmán, Y. Shen, and B. S. Shi, *Optica* **9**, 187 (2022).
- [18] T. Bauer, S. Orlov, U. Peschel, P. Banzer, and G. Leuchs, *Nat. Photonics* **8**, 23 (2014).
- [19] C. Hahn, Y. Choi, J. W. Yoon, S. H. Song, C. H. Oh, and P. Berini, *Nat. Commun.* **7**, 12201 (2016).
- [20] A. H. Dorrah, N. A. Rubin, A. Zaidi, M. Tamagnone, and F. Capasso, *Nat. Photonics* **15**, 287 (2021).
- [21] M. Born and E. Wolf, *Principles of Optics*, 7th ed. (Cambridge University Press, Cambridge, UK, 1999).
- [22] S. Daniel, K. Saastamoinen, T. Saastamoinen, I. Vartiainen, A. T. Friberg, and T. D. Visser, *Phys. Rev. Lett.* **119**, 253901 (2017).
- [23] C. P. Jisha, A. Alberucci, J. Beeckman, and S. Nolte, *Phys. Rev. X* **9**, 021051 (2019).
- [24] W. Zhu, H. Zheng, Y. Zhong, J. Yu, and Z. Chen, *Phys. Rev. Lett.* **126**, 083901 (2021).
- [25] A. Holleczeck, A. Aiello, C. Gabriel, C. Marquardt, and G. Leuchs, *Opt. Express* **19**, 9714 (2011).
- [26] G. Milione, H. I. Sztul, D. A. Nolan, and R. R. Alfano, *Phys. Rev. Lett.* **107**, 053601 (2011).
- [27] X. Yi, Y. Liu, X. Ling, X. Zhou, Y. Ke, H. Luo, S. Wen, and D. Fan, *Phys. Rev. A* **91**, 023801 (2015).
- [28] Z. C. Ren, L. J. Kong, S. M. Li, S. X. Qian, Y. Li, C. Tu, and H. T. Wang, *Opt. Express* **23**, 26586 (2015).
- [29] D. Naidoo, F. S. Roux, A. Dudley, I. Litvin, B. Piccirillo, L. Marrucci, and A. Forbes, *Nat. Photonics* **10**, 327 (2016).
- [30] V. D'Ambrosio, G. Carvacho, I. Agresti, L. Marrucci, and F. Sciarrino, *Phys. Rev. Lett.* **122**, 013601 (2019).
- [31] Z. Ji, W. Liu, S. Krylyuk, X. Fan, Z. Zhang, A. Pan, L. Feng, A. Davydov, and R. Agarwal, *Science* **368**, 763 (2020).
- [32] T. Giordani, A. Suprano, E. Polino, F. Acanfora, L. Innocenti, A. Ferraro, M. Paternostro, N. Spagnolo, and F. Sciarrino, *Phys. Rev. Lett.* **124**, 160401 (2020).
- [33] M. Liu, P. Huo, W. Zhu, C. Zhang, S. Zhang, M. Song, S. Zhang, Q. Zhou, L. Chen, H. J. Lezec, A. Agrawal, Y. Lu, and T. Xu, *Nat. Commun.* **12**, 2230 (2021).
- [34] Y. Shen, *J. Opt.* **23**, 124004 (2021).
- [35] C. He, Y. Shen, and A. Forbes, *Light Sci. Appl.* **11**, 205 (2022).
- [36] M. A. Alonso and M. R. Dennis, *Optica* **4**, 476 (2017).
- [37] M. R. Dennis and M. A. Alonso, *Philos. Trans. R. Soc., A* **375**, 20150441 (2017).
- [38] A. Vella and M. A. Alonso, *Opt. Lett.* **43**, 379 (2018).
- [39] R. Gutiérrez-Cuevas, S. A. Wadood, A. N. Vamivakas, and M. A. Alonso, *Phys. Rev. Lett.* **125**, 123903 (2020).
- [40] Y. Shen, Z. Wang, X. Fu, D. Naidoo, and A. Forbes, *Phys. Rev. A* **102**, 031501(R) (2020).
- [41] X. L. Wang, J. Ding, W. J. Ni, C. S. Guo, and H. T. Wang, *Opt. Lett.* **32**, 3549 (2007).
- [42] S. C. McEldowney, D. M. Shemo, R. A. Chipman, and P. K. Smith, *Opt. Lett.* **33**, 134 (2008).
- [43] D. S. Klinger, J. W. Lewis, and C. E. Randall, *Polarized Light in Optics and Spectroscopy* (Elsevier, Amsterdam, 1990).
- [44] A. M. Yao and M. J. Padgett, *Adv. Opt. Photonics* **3**, 161 (2011).
- [45] A. Aiello, P. Banzer, M. Neugebauer, and G. Leuchs, *Nat. Photonics* **9**, 789 (2015).
- [46] J. Wang, *Photonics Res.* **4**, B14 (2016).
- [47] D. L. P. Vitullo, C. C. Leary, P. Gregg, R. A. Smith, D. V. Reddy, S. Ramachandran, and M. G. Raymer, *Phys. Rev. Lett.* **118**, 083601 (2017).
- [48] Y. Shen, X. Wang, Z. Xie, C. Min, X. Fu, Q. Liu, M. Gong, and X. Yuan, *Light Sci. Appl.* **8**, 90 (2019).
- [49] X. Fang, H. Ren, and M. Gu, *Nat. Photonics* **14**, 102 (2020).
- [50] A. Chong, C. Wan, J. Chen, and Q. Zhan, *Nat. Photonics* **14**, 350 (2020).
- [51] K. Y. Bliokh, *Phys. Rev. Lett.* **126**, 243601 (2021).
- [52] J. Wang, J. Liu, S. Li, Y. Zhao, J. Du, and L. Zhu, *Nanophotonics* **11**, 645 (2022).
- [53] M. J. Padgett and J. Courtial, *Opt. Lett.* **24**, 430 (1999).
- [54] Y. Pan, X. Z. Gao, Z. C. Ren, X. L. Wang, C. Tu, Y. Li, and H. T. Wang, *Sci. Rep.* **6**, 29212 (2016).
- [55] S. M. Barnett, *J. Opt. B: Quantum Semiclassical Opt.* **4**, S7 (2002).